1-1-2010

Graphene doping to enhance the flux pinning and supercurrent carrying ability of a magnesium diboride superconductor

Xun Xu
University of Wollongong, xun@uow.edu.au

S X. Dou
University of Wollongong, shi@uow.edu.au

Xiaolin Wang
University of Wollongong, xiaolin@uow.edu.au

Jung Ho Kim
University of Wollongong, jhk@uow.edu.au

John A. Stride
School of Chemistry University NSW

See next page for additional authors

Graphene doping to enhance flux pinning and supercurrent carrying ability in magnesium diboride superconductor

X. Xu[1], S. X. Dou,[1] X. L. Wang[1], J. H. Kim[1], J. A. Stride[2], M. Choucair[2], W. K. Yeoh[3], R. K. Zheng[3], S. P. Ringer[3]

[1]Institute for Superconducting & Electronic Materials, University of Wollongong, Wollongong, NSW, 2522, Australia
[2]School of Chemistry, University of New South Wales, Sydney, NSW 2052, Australia
[3]Electron Microscope Unit, University of Sydney, NSW 2052, Australia

E-mail: shi_dou@uow.edu.au

Abstract

The effect of graphene doping on electromagnetic properties of MgB_2 has been examined in comparison with undoped MgB_2. It was found that graphene doping is more efficient than other forms of carbon doping for the improvement in the critical current density - field performance ($J_c(B)$), with little change in the transition temperature in MgB_2. An optimal enhancement in $J_c(B)$ was achieved for 3.7 at% graphene doped MgB_2 by a factor of 30 at 5 K and 10 T, compared to the un-doped MgB_2. It is found that spatial fluctuation in T_c is responsible for the flux pinning mechanism in grephene doped MgB_2.

(Some figures in this article are in colour only in the electronic version)

Substitutional chemistry can modify, in a controlled way, the electronic structures of superconductors and their superconducting properties, such as the transition temperature (T_c), critical current density (J_c), upper critical field (H_{c2}), and irreversibility field (H_{irr}). In particular, carbon containing dopants, including nano-meter sized carbon (nano-C), silicon carbide (SiC), carbon nanotubes (CNTs), hydrocarbons/carbohydrates, and graphite are effective means to enhance the J_c- field dependence and H_{c2} [1-11]. The graphene, a single-layered sheet of carbon atoms arranged in honeycomb lattice with great strength and excellent electrical conductivity, could be an effective dopant to incorporate carbon into MgB_2 and improve its Hi_{irr}, H_{c2} and the flux pinning properties without introduction of large amount of impurities which is a common problem for most dopants that have been studied so far. To our knowledge, there has been no report on the effects of graphene doping on the superconductivity of MgB_2, partly due to the unavailability of graphene on a large scale. Recently, high-throughput solution processing of large-scale graphene has been reported by a number of groups [12-17]. Here, we report the effect of graphene doping on the electromagnetic properties of MgB_2.

Based on the works of Choucair *et al.*[18], sufficient quantities of graphene were made available for doping the bulk MgB_2 samples. The lateral dimension of graphene sheet is about 0.1-10 μm with single atomic thickness estimates to be 4± 1 Å, and the elemental analysis of the residual graphene, as determined by XPS, was 86.4% C and 13.6% O by atomic composition (or by mass, 82.65% C and 17.35% O). The bulk MgB_2 samples were fabricated via a diffusion process. The crystalline boron powder (0.2 to 2.4 μm) 99.999% without and with graphene was prepared by ball milling with toluene medium. Then, the powders were dried in a vacuum oven to evaporate the medium. These powders were mixed and pressed into pellets. The pellets were then put into an iron tube filled with Mg powder (-325mesh 99%). The samples were sintered at 850°C for 10 hrs in a quartz tube; the heating rate was 5^oCmin^{-1} under high purity argon (Ar 99.9%) gas. The phase and crystal structure of all the samples were investigated by X-ray diffraction (XRD). T_c was defined as the onset temperature at which diamagnetic properties were observed. The magnetic J_c was derived from the width of the magnetization loop using Bean's model by a Physical Properties Measurement System (PPMS). Transport measurements for

resistivity (ρ) were done using a standard AC four probe method. In addition, $H_{c2}(T)$ and $H_{irr}(T)$ were defined as the fields where the temperature dependent resistance at constant magnetic field R(H_{c2}, T) = 0.9R_{ns} and R(H_{irr}, T) = 0.1R_{ns} with R_{ns} being the normal state resistance near 40 K. The hysteresis loops of the MgB_2 sample every 1.5 K in the 17- 35 K range. The symmetric hysteresis loops with respect to the magnetic field indicate the dominance of bulk pinning up to temperatures near T_c.

The common format $Mg(B_{1-x}C_x)_2$ with x=0, 0.037, and 0.087 was used. The composition of graphene doped MgB_2 were 0, 3.7, and 8.7 at%, and as such, the samples are designated as G000, G037, and G087, respectively. We demonstrate that the graphene doping results in a large enhancement of the critical current density (J_c) by over one order of magnitude in high magnetic fields. The J_c achieved is as high as 2.0×10^4 Acm^{-2} at 5 K and 8 T magnetic field for a graphene doping level of only 3.7 at%, with only a little drop in T_c . The magnitude of the improvement is greater than that by other form of carbon at the same doping level. attributable to the high efficiency of the single carbon sheet of graphene [19-22].

The lattice parameters, *a*, *c*, the ratio of *a/c,* grain size, strain, and full width at half maximum of the representative peak (110) calculated from the XRD patterns are shown in Table 1. Both the *a*-axis and *c*-axis parameters vary little with increasing graphene doping level of 3.7%, apart from G087 sample, which shows a notable decrease in the *a*-axis parameter, suggesting that carbon (C) likely substitutes into the boron (B) sites, leading to a slight drop in T_c (36.7 K) for the G087 sample. We also observed that the full width at half maximum (FWHM) of the (110) peak increases with increasing graphene doping level. Such a peak broadening is caused by both grain size reduction and an increase in lattice strain. The calculated results on grain size and lattice strain from a Williamson-Hall plot [23] are given in Table 1. Also, the T_c onset determined from the AC susceptibility measurement is 38.9 K for the un-doped sample, dropping only slightly to 37.7 and 36.7 K for the G037 and G087 samples, respectively.

Figure 1 shows the magnetic $J_c(B)$ curves at 5 K and 20K for all the samples, which were sintered at 850^{o}C for 10 hours. The $J_c(B)$ values for all the doped samples are higher than the un-doped sample at high fields. The sample G037 gives the highest J_c at high fields: J_c increases by a factor of 30 at 5 K for the field of 10 T, as compared to the un-doped sample, G000. Even though the J_c in the low field regime is depressed, a higher doping level (G087), still results in the rate of J_c dropping much slower than the un-doped sample,

clearly indicating strong flux pinning induced by the graphene doping. The most significant effect of graphene doping is the high effectiveness of graphene to improve flux pinning at lower doping levels, which distinguishes graphene from any other C containing dopants, for example, the J_c for G037 reached 20,000 A/cm^2 at 5 K and 8 T, exceeding or matching the best J_c resulting from dopants such as SiC, CNT, and carbohydrates at their optimal doping level of 10 at% [1,2,5-8], as well as nano-C at its optimal doping level of 5-6.4 at.% [3,4,9,10]. In the latter case, the T_c is substantially reduced to temperatures as low as 30 K. Compared to the graphite doped MgB_2 pellets prepared through the ball-milling and HIP the J_c of graphite doped MgB_2 is better than graphene doping at 5 K [11], but at 20K, the J_c for graphene doping is much better than graphite. For example, the J_c for the graphene doped MgB_2 at 20 K and 6 T is larger than that for graphite doped MgB_2 by a factor of 50 [11]. In comparison, low levels of graphene doping have little effect on T_c and cause only a very small increase in impurities, not compromising the significant enhancement in J_c in high fields by the degradation in low-field J_c, which is a common issue for all other C based dopants. In order to see the difference with other C based dopants, the same preparation route was applied to 5 at% nano-C doped sample and the resultant decrease in J_c at 20K can be seen in the figure 1, because the T_c for nano- C doped MgB_2 is only 34K.

Regarding the flux pinning mechanism, it is established that the core interaction, which stands for the coupling of the locally distorted superconducting properties with the periodic variation of the superconducting order parameter is dominant over the magnetic interaction for MgB_2 due to its large GL coefficient κ (~26 in MgB_2) [24]. The core interaction includes two types of mechanism: δTc and δl pinning. The δTc pinning refers to the spatial variation of the GL coefficient associated with disorder due to variation in the transition temperature T_c, while δl pinning is associated with the variation in the charge-carrier mean free path l near lattice defects [24]. According to the collective pinning model, the disorder induced spatial fluctuations in the vortex lattice can be clearly divided into different regimes depending on the strength of the applied field: single-vortex, small-bundle, large-bundle, and charge-density-wave (CDW)-type relaxation of the vortex lattice [25] The crossover field, B_{sb} is defined as a field separating single vortex regime into small bundles of vortices. Below B_{sb}, J_c is almost field independent. The B_{sb} as a function of reduced temperature ($t=T/T_c$) is described by the equation [25]:

$$B_{sb} = B_{sb}(0)\left(\frac{1-t^2}{1+t^2}\right)^{2/3} \quad (1)$$

for δT_c pinning,

$$B_{sb} = B_{sb}(0)\left(\frac{1-t^2}{1+t^2}\right)^{2} \quad (2)$$

for δl pinning.

To define the pinning mechanism in our grapheme doped the samples, the crossover field, $B_{sb,}$ as a function of temperature with graphene doped sample (G037) is plotted in figure 2 as red squares. B_{sb} is defined as a field where J_c drops by 5% only compared to J_c at zero field. It can be seen that the curve for δT_c pinning calculated from q. (1) is in a good agreement with the experimental data, whereas, the curve for δl pinning according to Eq. (2) does not fit to the experimental data. For polycrystalline, thin film, and single crystalline MgB_2 samples [25-27], it has been found that the dominant pinning mechanism is δT_c pinning, which is related to spatial fluctuation of the transition temperature while most C-doped MgB_2 samples displayed δl pinning mechanism [34] as a result of strong scattering and hence the shortening of the mean free path l owing to the presence of large amount of impurities in the doped samples. This is reflected by the significant increase in the residual resistivity [28]. The local strain was suggested to be one of potential pinning centres. However, we do not have strong evidence that the dominant pinning in the graphene doped MgB_2 is due to the local strain effect alone. In contrast, the graphene doping sets an exceptional example, following the δT_c pinning rather than δl pinning mechanism. This demonstrates the unique feature of the graphene doping. The amorphous phases can also act pinning centres, which is in favour for δT_c pinning. Although the graphene doped samples have a lot of defects these samples contain low concentration of impurities compared to the samples by other forms of carbon dopants. One of major differences of graphene doping from other dopants is that the samples are relatively pure as evidenced by the low resistivity (20 μΩ cm) in the grapheme doped samples. Normally, the resistivity in carbon doped MgB_2 ranges from 60 μΩ cm to as high as 300 μΩ cm. The high electrical connectivity is beneficial for J_c in low magnetic fields and high field performance; however we can not find any correlation between electrical con*n*ectivity with the J_c in the case here. The

graphene doped samples have higher resistivity than the un-doped MgB_2 sample (3 μΩ cm), indicating electron scattering caused by graphene doping levels. But, it should be pointed out that the increase in resistivity is much smaller than for any other forms of carbon doped MgB_2.

Figure 3 shows the **upper critical field, H_{c2}, and the irreversibility field, H_{irr},** versus the normalised T_c for all the samples. It is noted that both H_{c2} and H_{irr} are increased by graphene doping.

The mechanism for enhancement of J_c, H_{irr}, and H_{c2} by carbon containing dopants has been well studied. The C can enter the MgB_2 structure by substituting into B sites, and thus J_c and H_{c2} are significantly enhanced due to the increased impurity scattering in the two-band MgB_2 [29]. Above all, C substitution induces highly localised fluctuations in the structure and T_c, which have also been seen to be responsible for the enhancements in J_c, H_{irr}, and H_{c2} by SiC doping [1]. Furthermore, residual thermal strain in the MgB_2-dopant composites can also contribute to the improvement in flux pinning [30]. In the present work, the C substitution for B (up to 3.7 at.%) graphene doping is lower, from the table 1, the change of the *a*-parameter is smaller, according to Avdeev *et al* result [31], the level of C substitution, x in the formula $Mg(B_{1-x}C_x)$, can be estimated as $x=7.5 \times \Delta(c/a)$, where $\Delta(c/a)$ is the change in c/a compared to a pure sample. As both the *a*-axis and the *c*-axis lattice parameters determined from the XRD data showed little change within this doping range the level of carbon substitution is low at this doping level. This is in good agreement with the small reduction in T_c over this doping regime. At 8.7 at% doping, there is a noticeable drop in the *a*-axis parameter, suggesting C substitution for B, which is also consistent with the reduction in T_c. The source of C could be the edges of the graphene sheets, although the graphene is very stable at the sintering temperature (850^{o}C), as there have been reports of graphene formation on substrates at temperatures ranging from 870-1320^{o}C [32]. The significant enhancement in J_c and H_{irr} for G037 can not be explained by C substitution only.

The **microstructure** revealed by high resolution transmission electron microscope (TEM) observations show that G037 sample has grain size of 100-200 nm which is consistent with value of the calculated grain size in table 1. The graphene doped samples have relatively higher density of defects compared with the undoped sample as shown in the TEM images of figure 4(a) and (c). The density of such defects is estimated to be 1/3 areas of TEM images, indicating high density in the doped samples. In figures 4(b) it

should be noted that the order of fringes varies from grain to grain, indicates that the defect is due to highly anisotropic of the interface. Similar fringes have been reported in the MgB_2 [31] where these fringes were induced by tensile stress with dislocations and distortions which were commonly observed in the areas. As the graphene doped samples were sintered at 850^{o}C for 10 hrs, the samples are expected to be relatively crystalline and contain few defects. Furthermore, as already shown above the C substitution level is low in graphene doped samples. Thus, the large amount of defects and amorphous phases on the nanoscale can be attributed to the residual thermal strain between the graphene and the MgB_2 after cooling because the thermal expansion coefficient of graphene is very small while that for MgB_2 is very large and highly anisotropic [19,20]. The large thermal strain can create a large stress field, and hence structure defects and lattice distortion. These defects and distortions on the order of the coherence length, ξ, can play a role as effective pinning centres that are responsible for the enhanced flux pinning and J_c in the graphene doped MgB_2. The thermal strain-induced enhancement of flux pinning has also been observed in the SiC-MgB_2 composite as there is s noticeable difference in thermal expansion coefficient between MgB_2 and SiC [30].

In summary, the effects of graphene doping on the lattice parameters, T_c, J_c, and flux pinning in MgB_2 were investigated over a range of doping levels. By controlling the processing parameters, an optimised $J_c(B)$ performance is achieved at a doping level of 3.7 at.%. Under these conditions, J_c was enhanced by an order of magnitude at 8 T and 5 K while T_c was only slightly decreased. The strong enhancement in the flux pinning is argued to be attributable to a combination of C substitution for B and thermal strain-induced defects. Also, the evidence from collective pinning model suggests the δT_c pinning mechanism rather than the δl pinning for the graphene doped MgB_2, contrary to most doped MgB_2. The strong enhancement of J_c, H_{c2}, and H_{irr} with low levels of graphene doping is promising for large-scale MgB_2 wire applications.

Acknowledgments

We acknowledge support from the ARC (Australia Research Council) Project (DP0770205, LP100100440). The author would like to thank Dr. T. Silver for her helpful discussions. This work was supported by Hyper Tech Research Inc., OH, USA, and the University of Wollongong.

References

1. Dou S X, Soltanian S, Horvat J, Wang X L, Zhou S H, M. Ionescu, Liu H K, Munroe P, and Tomsic M, 2002 *Appl. Phys. Lett.* **81** 3419
2. Dou S X, Shcherbakova O, Yeoh W K, Kim J H, Soltanian S, Wang X L, Senatore C, Flukiger R, Dhalle M, Husnjak O, and Babic E, 2007 *Phys. Rev. Lett.* **98**, 097002-1
3. Ma Y, Zhang X, Nishijima G, Watanabe K, Awaji S, and Bai X, 2006 *Appl. Phys. Lett.* **88**, 072502
4. Jiang C H, Xu X, and Dou S X, 2008 *Supercond. Sci. Technol.* **21**(6), 5006
5. Kumakura H, Kitaguchi H, Matsumoto A, and Hatakeyama H, 2004 *Appl. Phys. Lett.* **84**, 3669-3671
6. Sumption M D, Bhatia M, Rindfleisch M, Tomsic M, Soltanian S, Dou S X, and Collings E W, 2005 *Appl. Phys. Lett.* **86**, 092507
7. Dou S X, Yeoh W K, Horvat J, and Ionescu M, 2003 *Appl. Phys. Lett.* **83**, 4996
8. Kim J H, Zhou S, Hossain M S A, Pan A V, and Dou S X, 2006 *Appl. Phys. Lett.* **89**, 142505
9. Wilke R H T, Bud'ko S L, Canfield P C, Finnemore D K, Suplinskas R J, and Hannahs S T, 2004 *Phys. Rev. Lett.* **92**, 217003
10. Häßler W, Herrmann M, Rodig C, Schubert M, Nenkov K, and Holzapfel B, 2003 *Supercond. Sci. Technol.* **21**, R17
11. Senkowicz B J, Giencke J E, Patnaik S, Eom C B, Hellstrom E E, and Larbalestier D C, 2005 *Appl. Phys. Lett.* **86**, 202502
12. Tung V C, Allen M J, Yang Y, and Kaner R B, 2009 *Nature Nanotech*. **4**, 25-29
13. Kim K S, Zhao Y, Jang H, Lee S Y, Kim J M, Kim K S, Ahn J H, Kim P, Choi J Y, and Hong B H, 2009 *Nature* **457**, 706-710
14. Hernandez Y, Nicolosi V, Lotya M, Blighe F M, Sun Z, De S, McGovern I T, Holland B, Byrne M, Gun'Ko Y K, Boland J J, Niraj P, Duesberg G, Krishnamurthy S, Goodhue R, Hutchison J, Scardaci V, Ferrari A C, and Coleman J N , 2008 *Nature Nanotech*. **3**, 563–568
15. Li D, Müller M B, Gilje S, Kaner R B, and Wallace G G , 2008 *Nature Nanotech*. **3**, 101–105

16. Li X, Wang X, Zhang L, Lee S, and Dai H, 2008 *Science* **319**, 1229–1232

17. Stankovich S, Dikin D A, Piner R D, Kohlhaas K A, Kleinhammes A, Jia Y, Wu Y, Nguyen S T, and Ruoff R S, 2007 *Carbon* **45**, 1558–1565

18. Choucair M, Thordarson P, and Stride J A, 2009 *Nature Nanotech*. **4**, 30-33

19. Mounet N, and Marzari N, 2005 *Phys. Rev. B* **71**, 205214

20. Röhrl J, Hundhausen M, Emtsev K V, Seyller Th, Graupner R, and Ley L, 2009 *Appl. Phys. Lett.* **92**, 201918

21. Neumeier J J, Tomita T, Debessai M, Schilling J S, Barnes P W, Hinks D G, and Jorgensen J D, 2005 *Phys. Rev. B* **72**, 220505

22. MacManus-Driscoll J L, 2008 *Nature Materials* **7**, 315

23. Williamson G K, and Hall W H, 1953 *Acta Metall.* **1**, 22-31

24. Finnemore D K, Ostenson J E, Bud'ko S L, Lapertot G, and Canfield P C, 2001 *Phys. Rev. Lett.* **86**, 2420

25. Qin M J, Wang X L, Liu H K, and Dou S X, 2002 *Phys. Rev. B* **65**, 132508

26. Prischepa S L, Della Rocca M L, Maritato L, Salvato M, Di Capua R, Maglione M G, and Vaglio R, 2003 *Phys. Rev. B* **67**, 024512

27. Shi Z X, Pradhan A K, Tokunaga M, Yamazaki K, Tamegai T, Takano Y, Togano K, Kito H, and Ihara H, 2003 *Phys. Rev. B* **68**, 104514

28. Kazakov S M, Puzniak R, Rogacki K, Mironov A V, Zhigadlo N D, Jun J, Soltmann Ch, Batlogg B, and Karpinski J, 2005 *Phys. Rev. B* **71**, 024533

29. Gurevich A, 2003 *Phys. Rev. B* **67**, 184515

30. Zeng R, Dou S X, Lu L, Li W X, Kim J H, Munroe P, Zheng R K, and Ringer S P, 2009 *Appl. Phys. Lett.* **94**, 042510

31. Avdeev M, Jorgensen J D, Ribeiro R A, Bud'ko S L, and Canfield P C, 2003 *Physica C* **387** 301-306

32. Coraux J, N'Diaye A T, Engler M, Busse C, Wall D, Buckanie N, Heringdorf F M, Gastel R, Poelsema B, and Michely T, 2009 *New J. Phys.* **11**, 023006

33. Blatter G, Feigel'man M V, Geshkenbein V B, Larkin A I and Vinokur V M, 1994 *Rev. Mod. Phys*. **66**, 1125

34. Wang J L, Zeng R, Kim J H, Lu L, and Dou S X, 2008 *Phys Rev. B* **77**, 174501

Table 1: The full width at half maximum (FWHM) of the (110) peak, the lattice parameters, and the transition temperature (T_c) for the MgB_2 samples, made with 0, 3.7, and 8.7 at% graphene doping via a diffusion process.

Sample	Lattice Constants			Grain Size (nm)	Strain (%)	FWHM (110) (°)	T_c (onset) (K)
	a (Å)	*c* (Å)	*c/a*				
G000	3.084(1)	3.525(1)	1.143(1)	216(10)	0.1198(188)	0.288	38.9
G037	3.082(1)	3.527(1)	1.144(1)	170(8)	0.1685(250)	0.400	37.7
G087	3.075(1)	3.525(1)	1.146(1)	171(11)	0.1782(330)	0.414	36.7

Figure Captions:

Figure 1: Critical current density as a function of magnetic field at 5 K and 20K for with and without graphene doped bulk samples. 5 at% nano-C doped sample for a comparable result at the same sample preparation route.

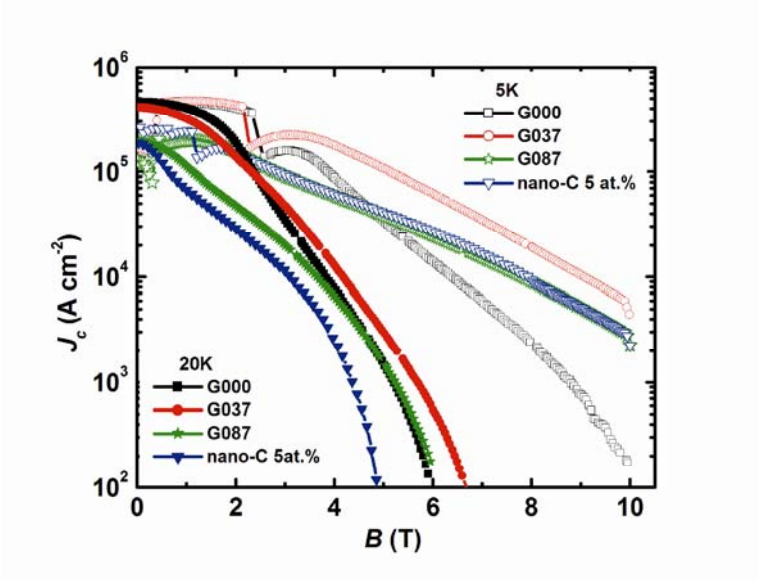

Figure 2: The crossover field B_{sb} as a function of temperature with graphene doped sample (G037).

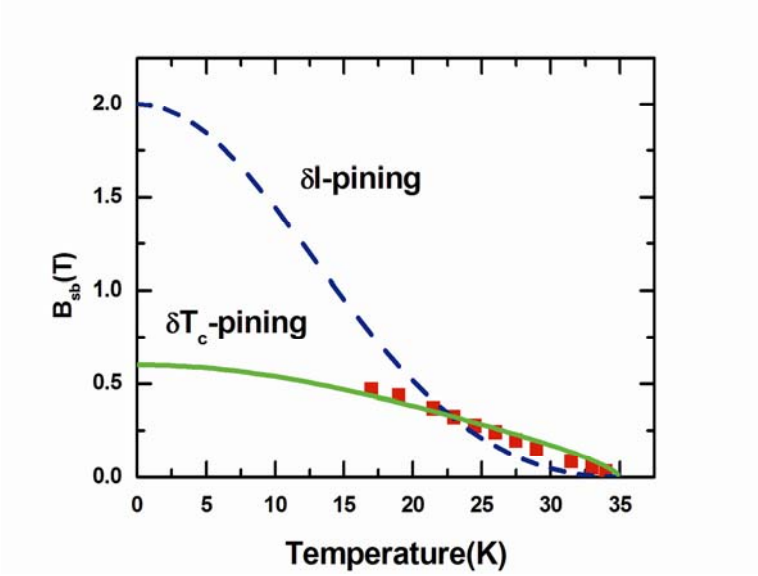

Figure 3: Upper critical field, H_{c2}, and irreversibility field, H_{irr}, versus normalised transition temperature, T_c, for all graphenedoped and undoped MgB_2 samples.

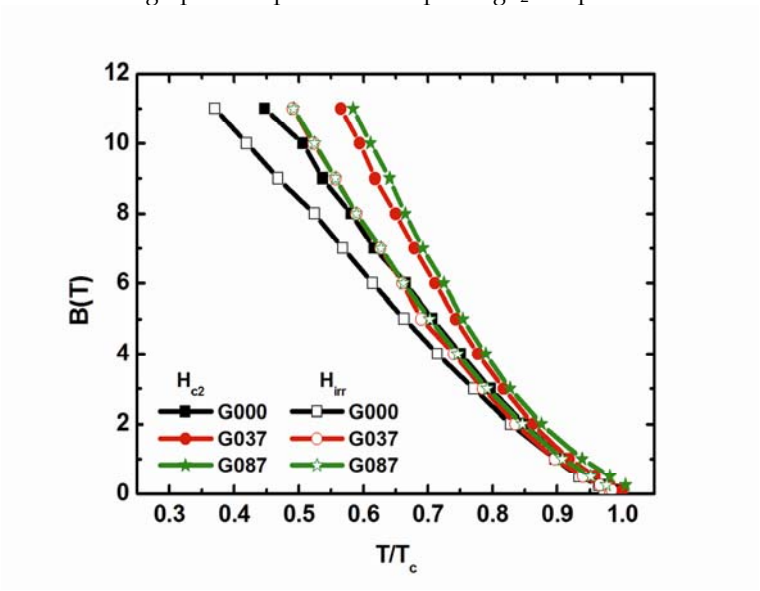

Fig. 11. (a) TEM image showing the defects with grains of the G037 sample with order of fringes varies between grains. Defects and fringes are indicated by arrow, and (b) HRTEM image of fringes. TEM images show large amount of defects and fringes can be observed in the graphene doped sample G037. (c) TEM image of the undoped sample for reference